Desalination and Water Treatment 318 (2024) 100383

Contents lists available at ScienceDirect

Desalination and Water Treatment

journal homepage: www.sciencedirect.com/journal/desalination-and-water-treatment/

Experimental evaluation of liquid circulation flow rate induced by an air-injection-type aerator

Kazuhiro Itoh[a,*], Norifumi Yoshida[b], Hideki Hayashi[b], Shogo Taguchi[a]

[a] University of Hyogo, 2167 Shosha, Himeji, Hyogo 671–2280, Japan
[b] Aience Co., Ltd., 21–7 Edobori-1chome, Nishi-ku, Osaka 550–0002, Japan

ARTICLE INFO

Keywords:
Wastewater treatment
Aerator
Liquid circulation flow
Diffuser

ABSTRACT

Despite previous research efforts, there is a lack of experimental data on liquid circulation flow rates, particularly in real-scale facilities. The study aims to fill this gap by proposing a momentum transfer model using a gas–liquid separation flow to estimate inner flow in a real-scale air-injection-type aerator. The liquid circulation flow rate was evaluated using velocity measurements. The air supply pressure and dissolved oxygen (DO) were determined. Experiments were performed at depths of 0.90, 1.30, and 1.75 m. The effect of the inner diffuser was investigated at each depth. The inner diffuser reduced the circulation flow rate but increased the vertical upward flow velocity. For the deepest condition (1.75 m), the inner diffuser reduced the air supply pressure and increased the overall oxygen transfer coefficient. Momentum analysis indicated a suppression effect of the air velocity at the aerator exit owing to the inner diffuser. This indicated that an increase in the gas holdup owing to the deceleration of the air velocity at the aerator exit reduced the air supply pressure owing to the reduction in downstream pressure. This study provides valuable insights into aeration system optimization, considering factors such as energy efficiency and oxygen transfer effectiveness.

1. Introduction

Sufficient air supply and agitation are crucial in biological wastewater treatment. Aerators are essential equipment in aerobic wastewater treatment plants [1]. Aeration systems are also essential to other industrial processes, such as airlift reactors [2] and bubble curtains [3], significantly influencing performance. The use of aerators is expanding to environmental purification and protection technologies [4] and the mass cultivation of microalgae [5,6].

However, the energy consumption associated with aeration is typically high, estimated to account for 15–20% of the total operating costs of aerobic fermentation [2]. Extensive effort has been made to improve oxygen transfer efficiency in aerator development. A large interfacial area and low bubble-rising velocity positively impact oxygen transfer efficiency. Therefore, membrane units have been employed rather than coarse bubble-type diffusers in wastewater treatment plants [7].

Insufficient oxygen supply arises in scenarios involving high organic nutrient and large biochemical oxygen demand (BOD) loads, such as in food wastewater. Siddiqui et al. [8] indicated that inadequate aeration results in low treatment efficiency and increased costs. Sediment decomposition owing to eutrophication accelerates hypoxia near the bottom of the tank. Anaerobic conditions generate hydrogen sulfide (H_2S) and malodorous gas [9–11].

To overcome these challenges, jet aerators have been developed to ensure sufficient oxygen supply. Agitation in a deep tank can be expected through momentum transfer from the strong air–liquid two-phase flow to the wastewater [12–16]. Compressed air or pumped liquid is vigorously mixed in the aerator and discharged into the tank. To develop an air-injection-type aerator, Iran et al. [17] evaluated the induced liquid flow through particle image velocimetry (PIV). Choi et al. [16] simulated agitation and fluid flow through computer fluid dynamics modeling. Burris and Little [18] and McGinnis and Little [19] compared the experimental oxygen transfer efficiency of an aerator with that of an analytical mass balance model. Recently, interest has been focused on the liquid circulation flow rate and gas holdup induced by air-injection-type aerators. An attempt to experimentally evaluate these values has been reported [20] for the airlift loop reactors, which has the downcomers. However, experimental data on liquid circulation flow rates remain limited, particularly in real-scale facilities for aerobic water treatment tanks because of the difficulty of evaluation.

Attempts have been made to solve the momentum equation to predict the liquid circulation flow rate during airlift reactor development. Liquid flow rate was determined from the motion of bubbles, defined by buoyancy and fluid drag after being released from the

* Corresponding author
E-mail address: itoh@eng.u-hyogo.ac.jp (K. Itoh).

https://doi.org/10.1016/j.dwt.2024.100383
Received 6 March 2024; Received in revised form 30 April 2024; Accepted 2 May 2024

sparger [3]. However, applying these results to apply to air-injection-type aerators is challenging because momentum transfer, denoting the acceleration of liquid, primarily occurs inside the device.

Airlift pumps are similar in terms of vertical two-phase flow exchange momentum in the device. However, their air flow rate is generally lower than that of jet aerators, and their riser tube is thinner and longer. Thus, the flow pattern and gas holdup, based on the airlift pump theory, do not align with the range of the aerator [21].

The novelty of this study is the experimental evaluation of the liquid circulation flow rate induced by a full-scale air-injected aerator in the aeration tank. This study proposes a momentum transfer model using gas–liquid separation flow to estimate the inner flow in a real-scale air-injection-type aerator. The influence of the inner components (i.e., the diffuser) on the velocity and gas holdup was investigated by substituting the liquid circulation flow rate evaluated using the three-dimensional velocity into the model. Finally, the tested aerator was applied in actual wastewater treatment facilities as a case study.

2. Nomenclature

A	Cross-sectional area [m^2]
C	Oxygen concentration [mg/L]
D	Outer cylinder diameter [m]
d	Nozzle diameter [m]
dP_d	Pressure loss at diffuser
G	Gap between floor and inlet of aerator [m]
g	Gravitational acceleration [m/s^2]
H	Depth of liquid [m]
H_d	Liftoff height [m] (depth from water surface to aerator exit)
J	Interfacial area density [1/m]
K	Correction coefficient of outlet pressure [-]
K_{La}	Overall oxygen transfer coefficient [1/h]
L	Length of aerator [m]
l	Vertical distance from the nozzle to the aerator exit [m]
M	Momentum [kg•m/s]
P	Pressure [Pa]
P_m	Measured air supply pressure [Pa]
Q	Flow rate [L/min]
Re	Reynolds number [-]
S_1	Drag coefficient [-]
T	Temperature [°C]
u	Velocity [m/s]
X_{tt}	Lockhart–Martinelli parameter
	Greek symbols
α	Gas holdup [-]
β	Aperture ratio [-]
δ	Liquid film thickness [m]
λ	Friction coefficient [-]
μ	Viscosity [Pa•s]
ρ	Density [kg/m^3]
τ_i	Interfacial shear stress [N/m^2]
τ_w	Wall shear stress [N/m^2]
ϕ_l	Two-phase frictional multiplier correlation
χ	Mass fraction of air
	Subscripts
1	Section at the exit of the air nozzle
2	Section at the aerator exit
g	Gas phase
l	Liquid phase
r	Radial coordinate
s	saturated
z	vertical coordinate
θ	Angular coordinate

3. Materials and methods

3.1. Experiment

Fig. 1 shows the layout of the experimental facility. An aerator (Aience Co., Ltd., Aquablaster AL-750) was mounted on the bottom of an underground tank (2 m wide, 2 m deep, and 16 m long). The tank was kept open to the atmosphere. Air was supplied using a blower

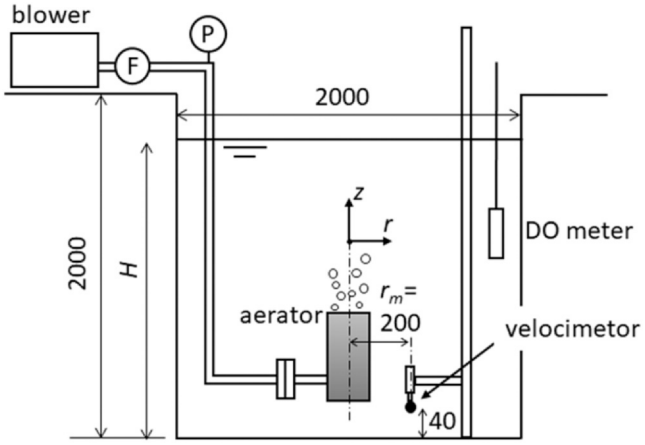

Fig. 1. Experimental facility.

(Hitachi Co., Ltd., VB-022-G, maximum air flow rate of 1.2 m^3/min) placed on the ground.

Fig. 2 shows the dimensions of the aerator. Air was released vertically upward from a nozzle with an inner diameter of d = 23 mm. The nozzle was housed in a 134 mm diameter (D) and 465 mm length (L) outer cylinder. The nozzle and outer cylinder were made of stainless steel. The distance between the nozzle and aerator exits was l = 315 mm. The gap between the aerator inlet and bottom of the tank was G = 50 mm. The injected air and drawn water flowed upward while colliding with the diffusers along the outer cylinder. Three sets of two types of diffusers, as shown in Fig. 2(b), were alternately inserted, totaling six units. Although these diffusers cannot rotate, their blades were designed to create a swirling flow and enhance agitation in the tank [22].

Table 1 lists the experimental conditions, including the distance from the aerator exit to the liquid surface, called the liftoff height H_d. Three taped water depths were tested, referred to as CASE 1, 2, and 3. Two types of tests were performed for each case, with (A) and without (B) the inner diffusers, to investigate the influence of the inner diffusers.

Air flow rate was measured using an ultrasonic flow meter (Aichi Tokei Denki Co., ltd., TRX50, measurement accuracy ±2%) installed on the horizontal pipe on the ground. Because the data $Q_{g,N}$ Nm^3/min was obtained under normal flow conditions, the actual flow rate Q_g m^3/min was converted using the following equation:

$$Q_g = \frac{101.33}{P_m + P_0} \cdot \frac{273.15 + T}{273.15} \cdot Q_{gN}, \tag{1}$$

where P_m is the air supply pressure measured using a pressure gauge (SMC Co., Ltd., ISE80, accuracy ±2.5%) installed on the horizontal pipe on the ground, P_0 is the base pressure (101.33 kPa), and T is the air temperature during the measurement.

Three-dimensional velocity was measured using an electromagnetic flow meter (JFE Advantec Co. Ltd, ACM3-RS, accuracy ±0.005 m/s). The measurement point was positioned 40 mm above the bottom and at a 200 mm radial distance (r_m) from the center of the aerator, as indicated by the black circle in Fig. 1.

In this study, the measurements of flow velocity and of dissolved oxygen (DO) were performed separately. The procedures of each were described below. At first, the procedure for velocity measurement was as follows: (i) The inverter-controlled blower was started from zero to the maximum frequency (60 Hz); (ii) Velocity was measured at the maximum air supply; (iii) The inverter frequency was reduced in 5 Hz or 10 Hz intervals, and velocity data were recorded after a waiting period of 3 min to achieve a steady state; (iv) These measurements were continued until the inverter frequency at which air supply was no longer possible. The instantaneous velocity values ($u_{l,r}$, $u_{l,\theta}$, $u_{l,z}$) were obtained at a 20 Hz sampling frequency over a 15 min duration. The

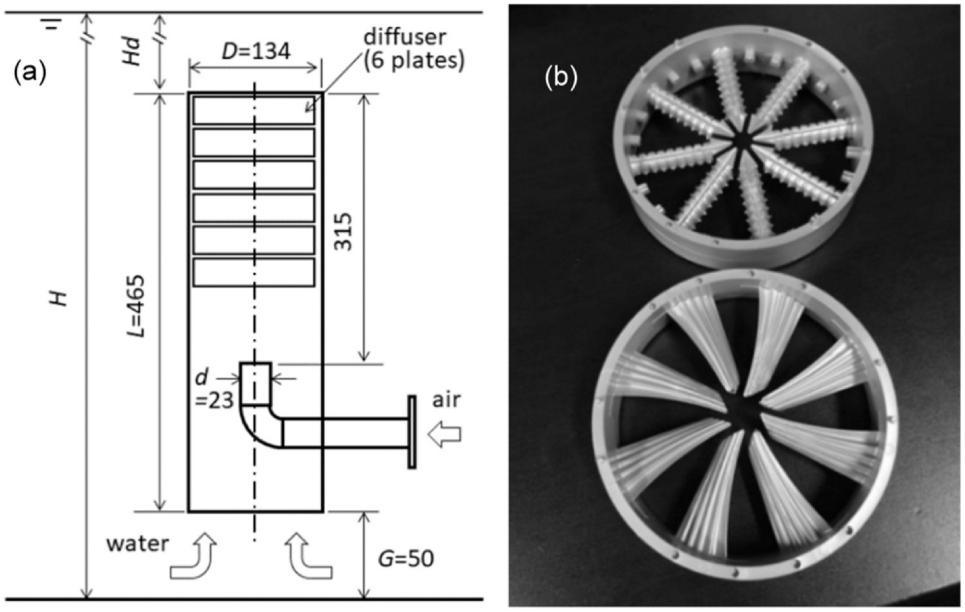

Fig. 2. (a) Dimensions of aerator and (b) photographs of inner diffuser.

Table 1
Experimental condition.

	H [m]	diffuser	H_d [mm]	DO-1 [m]	DO-2 [m]
CASE 1 A	0.90	Included	385	0.00	0.60
CASE 1B	0.90	Not included	385	0.00	0.60
CASE 2 A	1.30	Included	785	0.00	1.00
CASE 2B	1.30	Not included	785	0.00	1.00
CASE 3 A	1.75	Included	1235	0.75	1.50
CASE 3B	1.75	Not included	1235	0.00	1.50

circular liquid flow rate was calculated using the following equation:

$$Q_l = 2\pi \cdot r_m \cdot G \cdot u_{l,r}, \tag{2}$$

substituting the averaged value in the radial direction calculated for 16384 ($=2^{14}$) data points into $u_{l,r}$.

The DO measurements were performed on a different day from the velocity measurements to reduce the oxygen level in the tank. Two DO sensors (Iijima Electronics Co. Ltd., ID-150, accuracy ±0.1 mg/l) were installed near the side wall of the tank at the depths shown in Table 1. To measure the DO, the inverter frequency was raised from 0 Hz to 50 Hz rapidly. Time-series changes in the DO were recorded without waiting time. During data acquisition, the inverter frequency was fixed at 50 Hz. The overall oxygen transfer coefficient was calculated using the following equation:

$$K_L a = \frac{\ln \frac{C_s - C_1}{C_s - C_2}}{t_2 - t_1}, \tag{3}$$

where C_s is the saturation oxygen concentration at system temperature, and C_1 and C_2 are the DO values at times t_1 and t_2, respectively. The volume-weighted average values of the outputs of the two DO sensors were substituted into C_1 and C_2. The standard oxygen transfer coefficient at 20 °C was converted using the following equation:

$$K_{La(20)} = K_{La} \cdot \theta_T^{(20-T)}, \tag{4}$$

where T = 19.7–21.7 °C, and θ_T = 1.024.

For the value of velocity, liquid circulation flow rate and pressure, the standard deviation of fluctuations within the measurement time interval were displayed as an error bar in Figs. 4 and 5. For $K_{La(20)}$, the influences of accuracy of DO sensor (±0.1 mg/l) were shown by error bars in Fig. 7.

3.2. Analysis model

The injected air was assumed to rise to the center of the outer cylinder in a continuous phase because large bubbles were observed near the outlet of the aerator (see supplementary video). A separated flow model in an annular air–liquid two-phase flow was employed as shown in Fig. 3. The mass and momentum balance in the steady state between Sections 1 and 2 without a phase exchange is described as follows:

$$A\alpha_2 \rho_g u_{g,z2} - A\alpha_1 \rho_g u_{g,z1} = 0, \tag{5}$$

$$A(1-\alpha_2)\rho_l u_{l,z2} - A(1-\alpha_1)\rho_l u_{l,z2} = 0, \tag{6}$$

$$dM_g = -A_g dP - \rho_g g A_g dz - 2\pi r_i \tau_i dz - A_g dP_d, \tag{7}$$

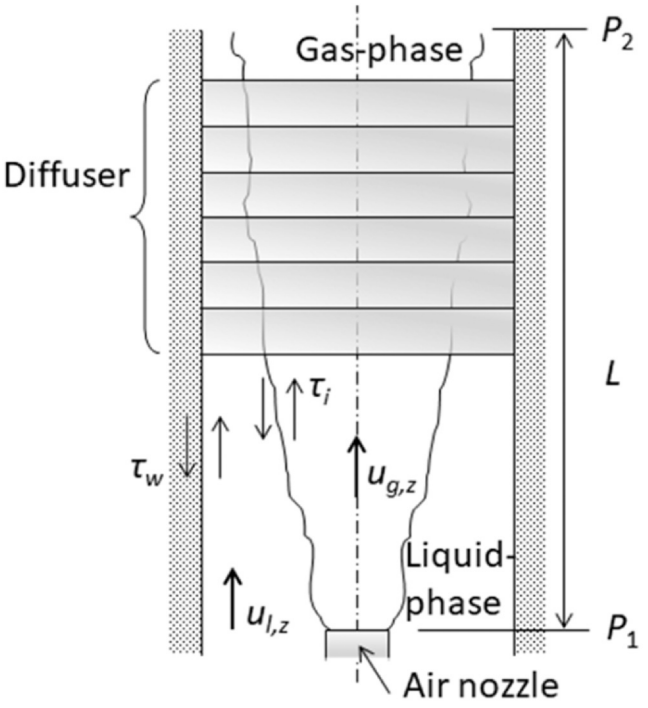

Fig. 3. Control volume for analysis of vertical upward two-phase annular flow.

$$dM_l = -A_l dP - \rho_l g A_l dz + 2\pi r_i \tau_i dz - 2\pi r_w \tau_w dz - A_l dP_d, \quad (8)$$

where α is the gas holdup, dP is the pressure gradient, r_i is the distance from the center of the aerator to the air–liquid interface, r_w (67 mm) is the outer cylinder radius, and dP_d is the pressure loss induced by the inner diffuser. The momentum variations, dM_g and dM_l, are expressed as follows:

$$dM_g = A\alpha_2 \rho_g u_{g,z2}^2 - A\alpha_1 \rho_g u_{g,z1}^2, \quad (9)$$

$$dM_l = A(1-\alpha_2)\rho_l u_{l,z2}^2 - A(1-\alpha_1)\rho_l u_{l,z1}^2. \quad (10)$$

Because only the liquid phase is in contact with the wall, the wall shear stress is determined as follows:

$$\tau_w = \frac{\lambda_l}{2}\rho_l u_{l,z}^2. \quad (11)$$

The friction loss coefficient λ_l is calculated by substituting the liquid velocity at the aerator outlet into the Blasius equation;

$$\lambda_l = 0.0791\,\mathrm{Re}^{-1/4}, \quad (12)$$

$$\mathrm{Re} = \frac{u_{l,z2}\cdot D}{\nu_l}. \quad (13)$$

The two-phase frictional multiplier ϕ_l is proposed for estimating the pressure drop. When the single-phase pressure drop for the liquid, and the two-phase pressure drops are described as $(dp/dz)_l$ and $(dp/dz)_F$ respectively, the following relationship is obtained:

$$\left(\frac{dP}{dz}\right)_F = \phi_l^2 \left(\frac{dP}{dz}\right)_l. \quad (14)$$

ϕ_l^2 is calculated using the Chisholm–Laird equation for turbulent flow in a smooth pipe [23] as follows:

$$\phi_l^2 = 1 + \frac{21}{X_{tt}} + \frac{1}{X_{tt}^2}, \quad (15)$$

where X_{tt} is the Lockhart–Martinelli parameter for turbulent flow, expressed as

$$X_{tt} = \left(\frac{1-x}{x}\right)^{0.9}\left(\frac{\rho_g}{\rho_l}\right)^{0.5}\left(\frac{\mu_g}{\mu_l}\right)^{0.1}. \quad (16)$$

x is the mass fraction of the gas phase, denoted as quality $x = \rho_g\alpha/\{\rho_g\alpha + \rho_l(1-\alpha)\}$. Using the above equations, the wall friction term in Eq. (8) was calculated as $2\pi r_w \tau_w dz = 2\pi r_w \tau_w \cdot l \cdot \phi_l^2$.

Interfacial shear stress can be evaluated using Wallis's equation [24] for turbulent flow, expressed as

$$\tau_i = \frac{\lambda_i}{2}\rho_g (u_{g,zm} - u_i)^2, \quad (17)$$

$$\lambda_i = \lambda_g \left[1 + 300\left\{\left(\frac{\delta}{D}\right) - \frac{5}{\mathrm{Re}_g}\sqrt{\frac{2}{\lambda_g}}\right\}\right], \quad (18)$$

where $u_{g,zm}$ and u_i are the average gas and interfacial velocities, respectively. In this study, these velocities are denoted by $u_{g,z2}$ and $u_{l,z2}$, respectively. The friction loss coefficient λ_g in gas was evaluated using Eqs. (12) and (13) by substituting $u_{g,z2}$ with $u_{l,z2}$. The average thickness of liquid film δ is calculated as $\delta = D(1-\sqrt{\alpha_2})/2$, assuming that the gas phase has a cylindrical shape, and its gas holdup can be represented by α_2. In the absence of waves and entrainment at the gas–liquid interface, the interfacial area density J, defined as the interfacial area per unit volume, can be expressed as

$$J = \frac{4\sqrt{\alpha_2}}{D}. \quad (19)$$

Therefore, the interfacial friction term in Eqs. (7) and (8) was determined as $2\pi r_i \tau_i dz = \tau_i \cdot J \cdot \pi D^2 \cdot l/4$.

The pressure loss dP_d induced by the inner diffuser was assumed to be approximated by the pressure loss for a perforated plate.

$$dP_d = \frac{1}{2}\rho u^2 S_1, \quad (20)$$

$$S_1 = \frac{\{0.707(1-\beta)^{3/8} + 1 - \beta\}^2}{\beta^2}, \quad (21)$$

where β is the aperture ratio [25]. In this study, these values are $\beta = 0.357$ for the wing-type diffuser, as shown in the bottom of Fig. 2(b), and $\beta = 0.487$ for the needle-type diffuser, as shown in the top of Fig. 2(b). The values at Section 2 were used for the gas and liquid velocity and gas holdup for evaluating dP_d.

Finally, the pressures in Sections 1 and 2 were assessed. The pressure at nozzle exit P_1 was calculated from P_m by considering the cumulative friction loss along the pipe and the local pressure losses due to the elbows and reducers. p_2 represents the pressure head, expressed as $P_2 = \rho_m g H_d$, where $\rho_m = \alpha_2\rho_g + (1-\alpha_2)\rho_l$ is the mixed density. Because the discharged bubbles would expand or spread before reaching the liquid surface of the tank, the actual pressure acting on the aerator exit differs from p_2. Subsequently, a factor K was introduced into the momentum balance analysis. In Eqs. (7) and (8), the pressure gradient was assumed as $dP = P_1 - K\cdot P_2 = P_1 - K\cdot\rho_m g H_d$.

Because the gas holdup at nozzle exit was constant $\alpha_1 = 0.0295$ in this experiment, four variables, u_{g2}, u_{l2}, α_2, and K, were considered in solving Eqs. (5)–(8). Eqs. (5)–(21) were translated into a Microsoft Excel worksheet. A solution was obtained using the generalized reduced gradient (GRG) nonlinear solution method by substituting the measured Q_g and Q_l. Convergence was considered achieved when the residual of the difference between the right and left hand sides decreased to 1×10^{-6}.

4. Results and discussion

4.1. Liquid circulation flow rate and velocity

Fig. 4(a) shows the liquid circulation flow rate Q_l, calculated from the average velocity $u_{l,r}$ in the radial direction. The horizontal axis represents the measured air flow rate Q_g at each tested inverter frequency.

The liquid circulation flow rate increased with the depth H. Compared with $Q_g \sim 1000$ L/min, $Q_l = 518$ L/min in Case 3B was larger than $Q_l = 495$ L/min in Case 2B or $Q_l = 359$ L/min in Case 1B. When the depth of the tank decreased, the influence of waves on the agitation of the liquid became apparent. The momentum transfer from the bubble to the liquid decreased owing to the short liftoff height H_d.

The inner diffuser reduced the liquid flow rate in all cases according to the local pressure drop. However, the maximum values of Q_g on the horizontal axis (i.e., at the maximum inverter frequency) in Cases 2 A and 3 A were greater than those in Cases 2B and 3B, in which the inner diffuser was not installed. The strict mechanism of the change in Q_g could not be explained. Nonetheless, the influence of the inner diffuser on the air supply pressure and injection rate is discussed in Section 3.3 based on the results of the momentum analysis.

Fig. 4(b) shows the average velocities in $u_{l,z}$. A vertical upward flow is crucial for preventing sediment growth at the bottom of the aeration tank. The values of $u_{l,z}$ increased when the inner diffuser was installed. In particular, a strong vertical flow occurred for $Q_g > 1000$ L/min in Cases 2 A and 3 A. Because the flow is no longer parallel to the bottom, the value of Q_l may be underestimated under these conditions. For instance, $u_{l,r}$ and $u_{l,z}$ were 0.055 and 0.029 m/s, respectively for $Q_g = 1356$ L/min in Case 3 A. Consequently, the flow angle with respect to the bottom was estimated to be $\tan^{-1}(0.029/0.055) = 28$ deg.

The influence of the inner diffuser on the circumferential velocity $u_{l,\theta}$, as shown in Fig. 4(c), is similar to that of Q_l. Thus, the diffuser reduced the velocity in the suction and circumferential directions and increased the velocity in the vertical direction.

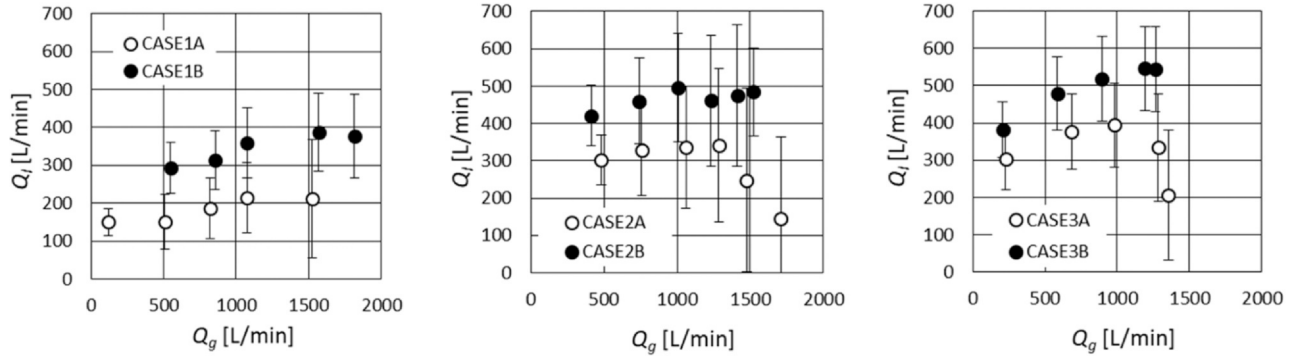

(a) Variation of Q_l

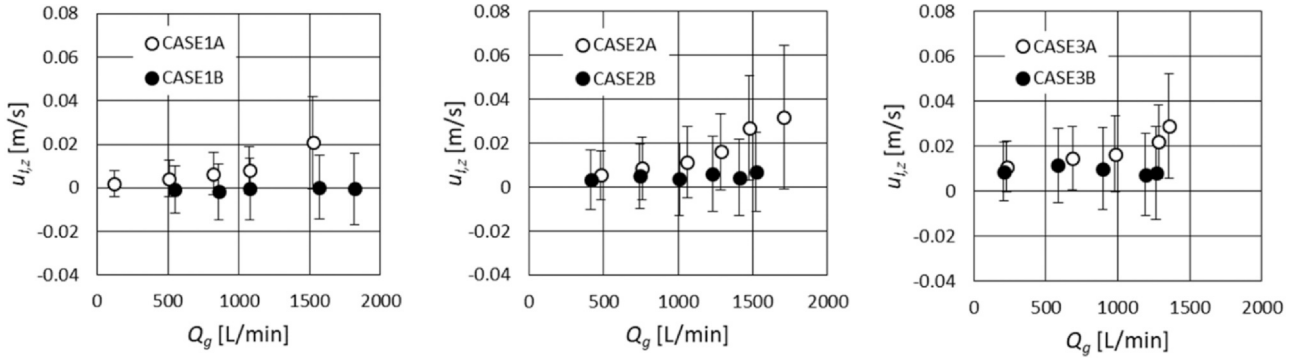

(b) Variation of $u_{l,z}$

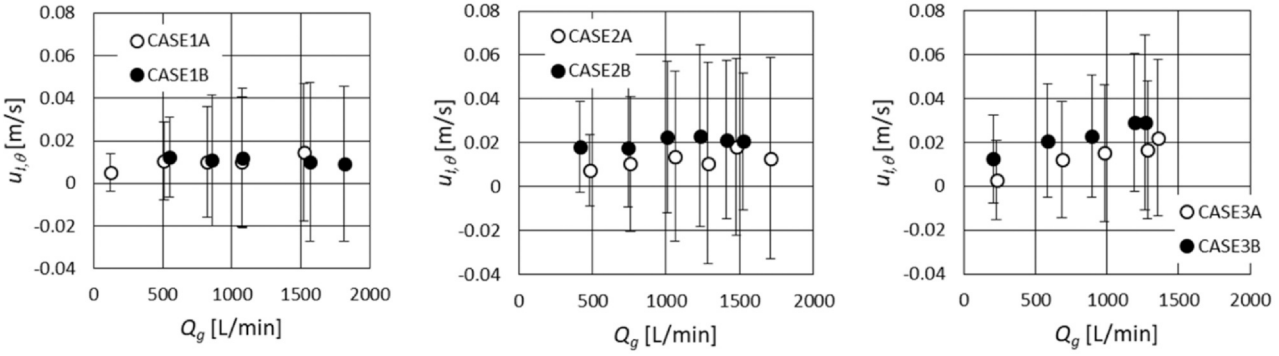

(c) Variation of $u_{l,\theta}$

Fig. 4. Variation of Q_l, $u_{l,z}$ and $u_{l,\theta}$ with Q_g.

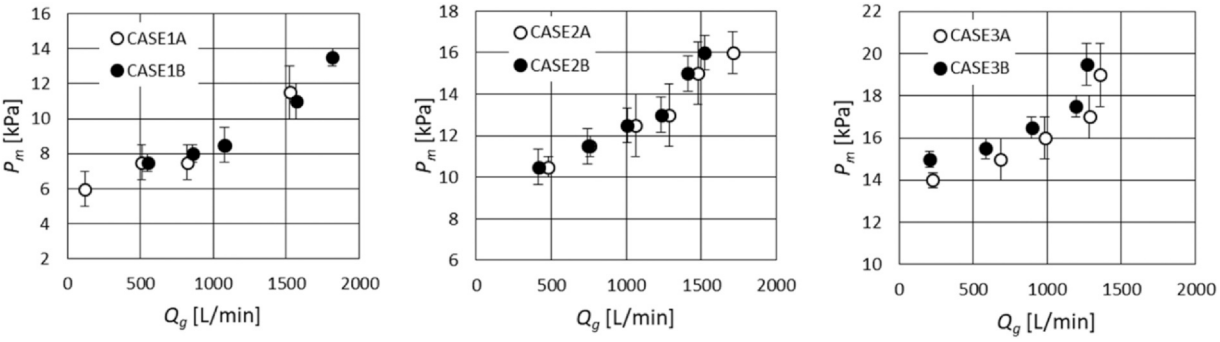

Fig. 5. Pressure in air supply pipe.

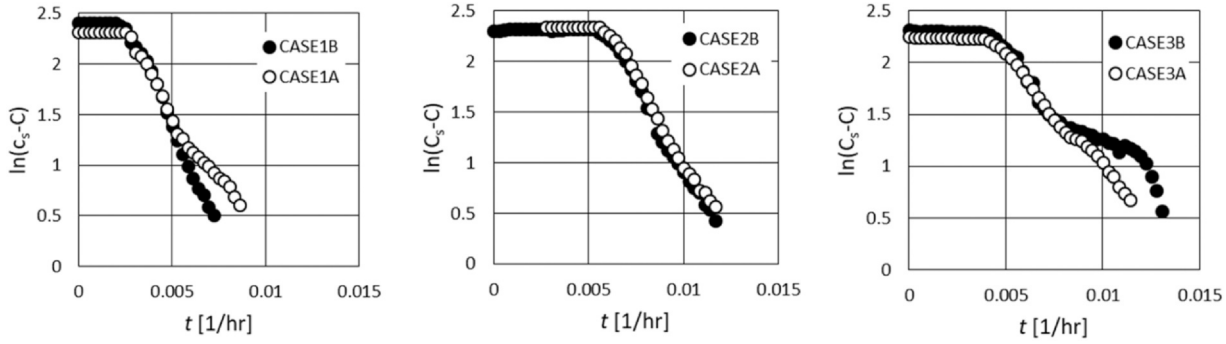

Fig. 6. Variation of oxygen deficit.

The air supply pressure P_m shown in Fig. 5 in this experiment was lower than that of the membrane-type aerator (for example, 30 kPa for Q_g = 13 L/min on Rizzardi's experiment [7]). The inner diffuser had relatively little effect on P_m in Cases 1 and 2. However, in Case 3, the pressure decreased when an inner diffuser was installed. Based on the results of the momentum analysis, as discussed in Section 3.3, one of the potential causes is a lower back pressure owing to a higher gas holdup after discharge from the nozzle.

4.2. Oxygen transfer

Fig. 6 presents the time-series data of oxygen deficits ($\equiv \ln(C_s - C)$). The inner diffuser affected the variation in $\ln(C_s - C)$ after 0.005 hr^{-1} in Case 1 and 0.007 hr^{-1} in Case 3. Fig. 7 shows the values of $K_{La(20)}$, calculated by substituting the slope of $\ln(C_s - C)$ into Eq. (3). Notably, the $K_{La(20)}$ values of the aerator in this study were larger than those of a venturi-type aerator ($K_{La(20)}$ = 12.8 h^{-1} at Q_l = 216 L/min) evaluated by Dong et al. [12].

In cases where the diffuser was not installed (i.e., Cases 1B, 2B, and 3B), $K_{La(20)}$ decreased with increasing depth. This trend is consistent with that observed by Wagner and Pöpel [26] and Gillot et al. [27]. In Cases 1 A, 2 A, and 3 A, the inner diffuser mitigated the variation in $K_{La(20)}$ with H. Thus, the difference between Cases 1 A and 3 A was smaller than that between Cases 1B and 3B. In particular, the value of $K_{La(20)}$ in the deepest condition (Case 3 A) exceeded that of Case 3B. The change in agitation caused by the inner diffuser affected the $K_{La(20)}$ value.

4.3. Analysis of momentum balance

The solution to Eqs. (5)–(8) can be obtained except for the minimum Q_l conditions in Cases 1 A, 3 A, and 3 B. Under these conditions, the momentum transfer after exiting the aerator (i.e., between the liftoff heights) was considered to be greater than that of other conditions. Fig. 8 shows the obtained solutions corresponding to the measured (Q_g, Q_l) values.

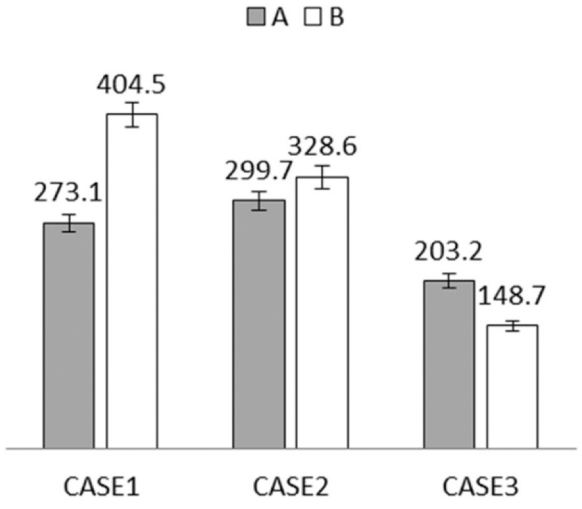

Fig. 7. $K_{La(20)}$ [1/h].

Fig. 8(a) shows the predicted gas holdup α_2 at the aerator exit. The α_2 values were larger than the inlet gas holdup of α_1=0.00295 and increased with Q_g. The reduction in the air velocity from $u_{g,z1}$ to $u_{g,z2}$ owing to the frictional and interfacial shear stress in the aerator increased the cross-sectional area of air phase $A{\cdot}\alpha_2$ in Eq. (5) and the α_2 values.

The triangular symbols in Fig. 8(a) represent the predicted values of air velocity $u_{g,z2}$ at the aerator exit. In the cases with the inner diffuser installed, as shown by the white triangles, $u_{g,z2}$ became lower than the black symbols. Because $u_{g,z1}$ at the nozzle exit was nearly the same for a similar Q_g between white and black, the local pressure drop at the inner diffuser enhanced the air-phase deceleration.

The air phase diameter at the aerator exit can be evaluated by $D\sqrt{\alpha_2}$. The value of $u_{g,z2}$ and $D\sqrt{\alpha_2}$ provide an outline of released bubble property. However, it is difficult to address the tendency of $K_{La(20)}$ from these values because the influences of the breakup or the dispersion of air bubble after exiting the aerator was not included in this analysis.

The correction coefficients of pressure K were nearly 1 for Cases 2B and 3B. However, the K values for Cases 2 A and 3 A were less than 1. The large gas holdup reduced the pressure head $K{\cdot}\rho_m g H_d$. The momentum balance substituting measured Q_g and Q_l induced that the mixed density of gas-liquid fluid between the liftoff height H_d would less than the value of ρ_m at the aerator exit for Case 2 A and 3 A. The reason is considered to be the deceleration of air bubble because of the breakup by the effect of diffuser. This may have caused the lower air supply pressure in Case 3 A compared with that in Case 3 B, as shown in Fig. 5. Moreover, the reduction in $K{\cdot}\rho_m g H_d$ may have also increased the maximum Q_g in Cases 2 A and 3 A, as shown in Fig. 4, owing to a reduced air nozzle back pressure. These prospects will be supported by the pressure measurements at the aerator exit in the future. And the present analytical results include errors due to neglecting the momentum transfer between the liftoff heights. Incorporating a model for this section would reduce the error, especially for low Q_l conditions.

4.4. Case study

A cut vegetable manufacturing plant in Iwate Prefecture, Japan, has a private wastewater treatment facility with seven 31.5 m^3 primary aeration tanks. An overview of these facilities is provided in the Supplementary Information. The average flow is 300 m^3/d (0.08 mgd). A total of 35 units, five units in each tank, of the aerator in this study (AL-750, inner diffuser included) were installed. For preaeration, 31 small-sized aerators (AS-250, 68 mm in diameter and 176 mm in height) were installed in the 101.3 m^3 flow-control tank upstream of the primary tanks. The facility also has a 40.3 m^3 sedimentation tank downstream of the primary tanks. The air flow rate is 3.75 m^3/min for

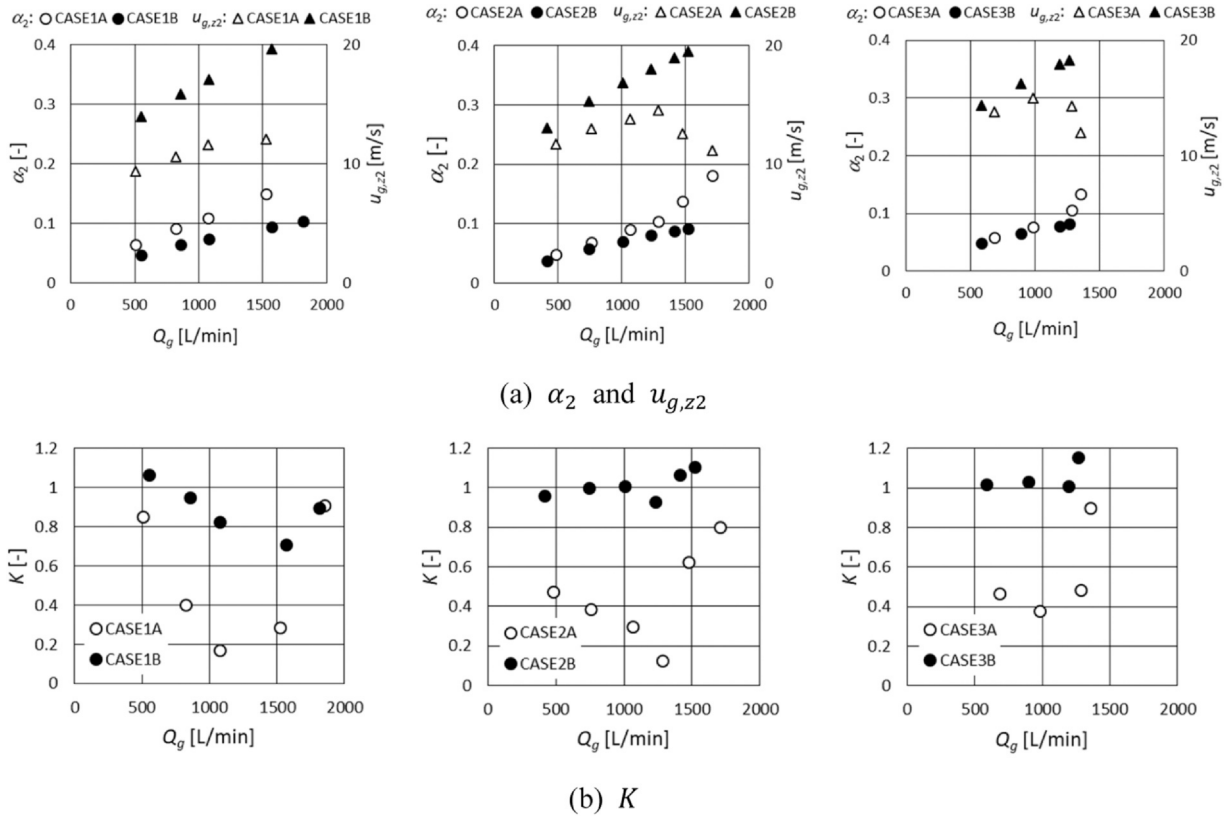

Fig. 8. Prediction of α_2, $u_{g,2}$ and K.

each aeration tank and 7.75 m^3/min for the flow-control tank. Table 2 lists the wastewater characteristics, all of which meet the Japanese effluent standards.

The next facility treats kitchen wastewater (60 m^3/d (0.02 mgd) from food and dish washing in the cafeteria of a measurement hardware manufacturing factory in Kanagawa Prefecture, Japan. Twenty-five AL-750 are installed in five aeration tanks, each with a capacity of 23.8 m^3. A small 6th aeration tank (10 m^3), a sedimentation tank (7.8 m^3), and an effluent flow-control tank (4.0 m^3) are installed downstream of the five aeration tanks. Two AL-750 units and five AS-250 units are installed in the 6th aeration tank and effluent flow-control tanks, respectively. The total air flow rate supplied to the 1st to 3rd aeration tanks is controlled at 13.5 m^3/min. The total air flow rate supplied to the 4th to 6th aeration tanks and effluent flow-control tank is 12.3 m^3/min.

Table 3 summarizes the results. In the previous equipment, organic fats and oils treatment was incomplete, generating foul odors. After installing the AL-750 units, the residues of the organic material were reduced, and odors were resolved. The sludge disposal interval was drastically extended.

Table 3
Wastewater characteristics on kitchen of cafeteria of manufacturing factory. Unit: [mg/l].

	BOD	COD	SS	n-hex
Influent	1000	500	1200	400
Effluent	40	40	50	< 1.0

5. Conclusions

This study investigated the influence of the inner diffuser incorporated in an air-injection-type aerator across three aeration tank depths. The results limited for a range of the experimental conditions and the model of aerator was concluded as below.

The inner diffuser reduced the liquid circulation flow rate up to 49%. However, the vertical component of velocity increased when the diffuser was installed. The maximum increase in vertical velocity was achieved in Case 1 A, which was 75 times greater than that of Case 1B. Under the deepest condition (Case 3 A), the inner diffuser reduced the air supply pressure up to 13%.

Table 2
Wastewater characteristics on the cut vegetable manufacturing plant. Unit: [mg/l].

	BOD	COD	SS	n-hex	T-N	T-P
Influent	920	830	960	8.7	100	14
Effluent	7.0	22	7	1	4.8	0.5
Effluent standards	≤160	≤160	≤200	≤5	≤120	≤16

BOD = biochemical oxygen demand.
COD = chemical oxygen demand.
SS = suspended solids.
n-hex = normal hexane
T-N = total nitrogen
T-P = total phosphorous

For oxygen transfer, the presence of an inner diffuser reduced the sensitivity of $K_{La(20)}$ to depth. $K_{La(20)}$ in Case 3 A was 1.4 times greater than that in Case 3 B, where the diffuser was not included.

The air velocity and pressure at the aerator exit were evaluated by substituting the measured Q_g and Q_l values into the momentum balance equation for annular two-phase flow. The local pressure drop in the inner diffuser reduced the air velocity and increased the gas holdup at the aerator exit. A higher gas holdup may reduce the air supply pressure.

This study provides valuable insights into the design and optimization of air-injection-type aerators. The potential benefits include the reduction in liquid circulation flow rate, improved oxygen transfer efficiency, and energy optimization through careful consideration of inner diffuser characteristics.

Funding

This work was supported by an innovation grant from City of Osaka, H28.

CRediT authorship contribution statement

Kazuhiro Itoh: Writing – original draft, Investigation, Data curation, Conceptualization. **Norifumi Yoshida:** Supervision, Project administration. **Hideki Hayashi:** Validation, Supervision. **Shogo Taguchi:** Validation, Software.

Declaration of Generative AI and AI-assisted technologies in the writing process

Statement: During the preparation of this manuscript, the authors used Deep L for Japanese to English translation. After using this service, the authors reviewed and edited the content as needed and take full responsibility for the content of the publication.

Data availability

Data will be made available on request.

Declaration of Competing Interest

The authors declare that they have no known competing financial interests or personal relationships that could have appeared to influence the work reported in this paper.

Acknowledgment

The authors express their sincere appreciation to Mr. Fuya Yoshimura and Mr. Tomoaki Shimada of the University of Hyogo.

Appendix A. Supporting information

Supplementary data associated with this article can be found in the online version at doi:10.1016/j.dwt.2024.100383.

References

[1] Gu Y, Li Y, Yuan F, Yang Q. Optimization and control strategies of aeration in WWTPs: a review. J Clean Prod 2023;418:138008. https://doi.org/10.1016/j.jclepro.2023.138008.
[2] Behin J, Amiri P. A review of recent advantages in airlift reactors technology with emphasis on environmental remediation. J Environ Manag 2023;335:11756. https://doi.org/10.1016/j.jenvman.2023.117560.
[3] Zafeirakou A, Pechlivanidis G, Koutitas C. Theoretical analysis and experimental investigation of air-bubble-stream-induced water circulation. Eur-Mediterr J Environ Integr 2023;8:275–86. https://doi.org/10.1007/s41207-023-00376-0.
[4] Nakata A, Yanobu T, Yamagishi M, Hosoki Y. Model experiments on water treatment and oxgen transfer of air lifting tower placed in bottom of reservior. J Jpn Soc Exp Mech 2010;37(2):90–5.
[5] López-Rosales L, Sánchez-Mirón A, Contreras-Gómez A, García-Camacho F, Battaglia F, Zhao L, Molina-Grima E. Characterization of bubble column photobioreactors for shear-sensitive microalgae culture. Bioresour Technol 2019;275:1–9. https://doi.org/10.1016/j.biortech.2018.12.009.
[6] Itoh K, Taguchi S, Yoshida N, Yamamoto T, Maeda K. Enhanced triacylglycerol accumulation in open cultivation of microalgae using an air self-sufficient aerator. Bioresour Technol Rep 2022;17:100916. https://doi.org/10.1016/j.biteb.2021.100916.
[7] Rizzardi I, Bottino A, Capannelli G, Pagliero M, Costa C, Matteucci D, Comite A. Membrane bubble aeration unit: experimental study of the performance in lab scale and full-scale systems. J Membr Sci 2023;685:121927. https://doi.org/10.1016/j.memsci.2023.121927.
[8] Siddiqui MI, Hasan R, Farooqi IH, Basheer F. Aeration control strategy design based on dissolved oxygen and redox potential profiles for nitrogen and phosphorus removal from sewage in a sequencing batch reactor. J Water Proc Eng 2022;50:103259. https://doi.org/10.1016/j.jwpe.2022.103259.
[9] Rosenberg R, Diaz RJ. Sulfur Bacteria (Beggiatoa spp.) Mats Indicate Hypoxic Conditions in the Inner Stockholm Archipelago. AMBIO 1993;22(1):32–6https://www.jstor.org/stable/4314034.
[10] Lutz M, Davidson S, Stowe D. Making Less Scents With Good Reason. Water Environ Technol 1995;7(6):52–7https://www.jstor.org/stable/24664800.
[11] Ali J, Yang Y, Pan G. Oxygen micro-nanobubbles for mitigating eutrophication induced sediment pollution in freshwater bodies. J Environ Manag 2023;331:117281. https://doi.org/10.1016/j.jenvman.2023.117281.
[12] Dong C, Zhu J, Wu X, Miller CF. Aeration efficiency influenced by venturi aerator arrangement, liquid flow rate and depth of diffusing pipes. Environ Technol 2012;33(11):1289–98. https://doi.org/10.1080/09593330.2011.620986.
[13] Anker Y, Mualem D, Gimburg A, Koplon B, Gur E, Nocham A, Rosental Y. Application of an innovative venturi type aeration array as part of the restoration and upgrading of an obsolete wastewater treatment plant. APCBEE Procedia 2014;10:120–5. https://doi.org/10.1016/j.apcbee.2014.10.028.
[14] Chipongo K, Khiadani M. Reoxygenation by free, wall-supported, and plate-supported rectangular jets plunging into a quiescent pool. J Environ Eng 2017;143(8):04017031. https://doi.org/10.1061/(ASCE)EE.1943-7870.0001233.
[15] Radkevich M, Abdukodirova M, Shipilova K, Abdullaev B. Determination of the optimal parameters of the jet aeration. Earth Environ Sci 2021;939(1):012029. https://doi.org/10.1088/1755-1315/939/1/012029.
[16] Choi B, Jeong T-Y, Lee S. Application of jetventurimixer for developing low-energy-demand and highly efficient aeration process of wastewater treatment. Heliyon 2022;8:e11096. https://doi.org/10.1016/j.heliyon.2022.e11096.
[17] Iran EN, David ZZ. Air injection in water with different nozzles. J Environ Eng 2008;134(4):283–94. https://doi.org/10.1061/(ASCE)0733-9372(2008)134:4(283).
[18] Burris VL, Little JC. Bubble dynamics and oxygen transfer in a hypolimnetic aerator. Water Sci Technol 1998;37(2):293–300. https://doi.org/10.1016/S0273-1223(98)00036-5.
[19] McGinnis DF, Little JC. Bubble dynamics and oxygen transfer in a speece cone. Water Sci Technol 1998;37(2):285–92. https://doi.org/10.1016/S0273-1223(98)00035-3.
[20] Xu X, Zhang Y. Hydrodynamics and mass transfer in an airlift loop reactor: comparison between using two kinds of spargers. Processes 2024;12:35. https://doi.org/10.3390/pr12010035.
[21] de Cachard F, Delhaye JM. A slug-churn flow model for small-diameter airlift pumps. Int J Multiph Flow 1996;22(4):627–49. https://doi.org/10.1016/0301-9322(96)00003-1.
[22] N. Yoshida, K. Itoh, Bubble Generating Device for Sewage Purification, WO 2018/151171 A1 (2018).
[23] Zhang W, Hibiki T, Mishima K. Correlations of two-phase frictional pressure drop and void fraction in mini-channel. Int J Heat Mass Transf 2010;53:453–65. https://doi.org/10.1016/j.ijheatmasstransfer.2009.09.011.
[24] Mascarenhas N, Lee H, Mudawar I. Experimental and computational investigation of interfacial shear along a wavy two-phase interface. Int J Heat Mass Transf 2015;85:265–80. https://doi.org/10.1016/j.ijheatmasstransfer.2015.01.096.
[25] Idelchik IE. Handbook of Hydraulic Resistance. fourth ed.., New York: Begell House, Inc; 2007. p. 592.
[26] Wagner MR, Pöpel HJ. Oxygen transfer and aeration efficiency - Influence of diffuser submergence, diffuser density, and blower type. Water Sci Technol 1998;38(3):1–6. https://doi.org/10.1016/S0273-1223(98)00445-4.
[27] Gillot S, Capela-Marsal S, Roustan M, Héduit A. Predicting oxygen transfer of fine bubble diffused aeration systems-model issued from dimensional analysis. Water Res 2005;39(7):1379–87. https://doi.org/10.1016/j.watres.2005.01.008.